This is the pre-review version of the paper
published in

J. Mol. Model., 19, 5457-5467

The final version of this paper is available in
http://dx.doi.org/10.1007/s00894-013-2045-z

Evaluation of density functional methods on the geometric and energetic descriptions of species involved in Cu^{+}-promoted catalysis

Carlos E. P. Bernardo[1], Nicholas P. Bauman[2], Piotr Piecuch[2], and Pedro J. Silva[1]*

[1]REQUIMTE, Faculdade de Ciências da Saúde, Univ. Fernando Pessoa, Rua Carlos da Maia, 296, 4200-150 Porto-Portugal

[2] Department of Chemistry, Michigan State University, East Lansing, Michigan 48824, USA

*pedros@ufp.edu.pt

Abstract: We have evaluated the performance of fifteen density functionals of diverse complexity on the geometry optimization and energetic evaluation of model reaction steps present in the proposed reaction mechanisms of Cu(I)-catalyzed indole synthesis and click chemistry of iodoalkynes and azides. The relative effect of the Cu^+ ligand on the relative strength of Cu^+-alkyne interactions, and the strong preference for a π-bonding mode is captured by all functionals. The best energetic correlations with MP2 are obtained with PBE0, M06-L, and PBE1PW91, which also provide good quality geometries. Furthermore, PBE0 and PBE1PW91 afford the best agreement with the high-level CCSD(T) computations of the deprotonation energies of Cu^+-coordinated eneamines, where MP2 strongly disagrees with CCSD(T) and the examined DFT functionals. PBE0 also emerged as the most suitable functional for the study of the energetics and geometries of Cu^+ hydrides, while at the same time correctly capturing the influence of the Cu^+ ligands on the metal reactivity.

Keywords: DFT; Cu(I) complexes; MP2; CCSD(T)

Introduction

Transition metal-catalyzed organic reactions have found a vast number of applications in synthesis, including C-C coupling[1], homogeneous hydrogenation[2], and C-H bond functionalization[3]. The role of the transition metal in the reaction mechanism may be quite varied: it may act as a Lewis acid–(as in the classical $FeCl_3$-catalyzed Friedel-Crafts acylation), polarize metal-C bonds (yielding carbon-based nucleophiles, or even carbanionic species), or undergo sequential oxidative addition and reductive elimination (e.g. the Pd-catalyzed Suzuki coupling reaction). Furthermore, *d*-block metal complexes often present both empty and filled anti-bonding orbitals of comparable energies, which enable them to interact with π-bonds (and even with σ-bonds) with "carbene-like" reactivity[4]. In spite of the importance of these reactions, their mechanisms remain largely speculative, and thorough theoretical studies are not as abundant as those of purely organic reactions. We expect that a deeper understanding of this chemistry will enable the development of improved catalysts and reaction conditions, and expand the chemical space available for exploration.

We are particularly interested in Cu(I)-based catalysis, which has recently been applied to C-C bond formation through C-H functionalization[5], annulation reactions of iodoacetylenes with organic azides[6], and to finely tailored aldol reactions[7]. In each case, the reactions have been elegantly designed to provide simple and effective one-pot syntheses of multisubstituted indoles, 1,4,5- substituted 1,2,3-triazoles, and quaternary stereocenters, respectively. This set of syntheses encompasses a wide range of reaction conditions: either requiring Cu(I) ligands for full reactivity[5,6] or bare Cu(I)-organometallic[7], different ligand requirements (e.g. phenanthroline is required in Ref. 5

but inhibits catalysis in Ref. 6), and reaction temperatures (ranging from -20ºC[7] to room temperature[6] and 100 ºC[5]) which reflect widely different activation energies among the reactions. Although several mechanistic proposals have been put forward for each of these syntheses, none of them has been subjected to a theoretical study. Computational studies on the annulation of terminal acetylenes with organic azides[8,9] do exist, but their relevance for the annulation of iodoacetylenes[5] is not certain, as the product profile seems to favor a different reaction pathway.

Density functional theory (DFT) is a relatively inexpensive way to include electron correlation in quantum chemistry computations. Although it can be shown that an exact functional relating the electron density to the ground-state wavefunction exists, the form of this functional is unknown. Many different approximations to the exact functional have been developed, some of which afford exceptionally good results for some properties in some systems, though not for all properties and all possible systems[10]. Traditionally, the B3LYP[11–13] functional has been shown to be a robust choice for a wide range of chemical problems, and used as the "default" functional. The increase in computational power and the development of faster algorithms now make a more sensible functional choice feasible in many circumstances, allowing for the fast computation of simplified reaction pathways with many different functionals in relatively short times. We have evaluated the performance of a large number of density functionals on the geometry optimization and energetic evaluation of model reaction steps present in the proposed reaction mechanisms of Cu(I)-catalyzed indole synthesis and click chemistry of iodoalkynes and azides. Comparison of these results with high-level MP2 and CCSD(T) computations identify the most suitable functionals for each of these studies.

Computational methods

The geometries of every molecule described were optimized at the MP2 level and with each of the tested density functionals. We used 15 functionals in total - one GGA functional (PBEPW91[14,15]), eight hybrid-GGA functionals (B3LYP[11–13], B3PW91[11,14], B97-1[16], B97-2[17], BHHLYP (50% HF exchange + plus 50% B88[18] exchange, with LYP correlation), PBE0[19], PBE1PW91[14,15], and X3LYP[20]), three meta-GGA functionals (TPSS[21,22], TPSSm[23], and M06-L[24]) and three meta-hybrid GGA functionals (TPSSh[25], M06[26], and M06-HF[27]). Autogenerated delocalized coordinates[28] were used in geometry optimizations performed with 6-31G(d)[29,30] for all elements except for Cu and I, which used the SBKJ VDZ[31] basis set was used in combination with the SBKJ pseudo-potential[31] for the inner shells corresponding to the (1s2s2p) core of Cu and the (1s2s2p3s3p3d4s4p4d) core of I. Single-point energies of the DFT-optimized geometries obtained with each density functional were then calculated using the same functional with two different basis sets: BS1 used 6-311G(2d,p)[32–34] for all elements except Cu, which used the s6-31G* basis set developed by Swart *et al.*[35]; BS2 used 6-311+G(2d,p)[32–34,36] for all elements except I and Cu, which used 6-311G(d,p)[37] or aug-cc-pVDZ[38], respectively, in conjunction with the SBKJ pseudo-potential. MP2 single-point energies were computed with the MP2 geometries using aug-cc-pVDZ[38–40] and aug-cc-pVTZ[38–41] basis sets combined with the SBKJ pseudo-potential for the core electrons of Cu and I. In order to evaluate the accuracy of the MP2 and DFT single-point energies for the deprotonation of Cu^{+}-coordinated eneamines, we ran additional coupled-cluster[42] calculations for the MP2-optimized 6c, 7c, 6d, and 7d structures using the conventional coupled-cluster method with singles, doubles, and non-iterative triples (CCSD(T))[43] employing the restricted Hartree-Fock (RHF) reference. The CCSD(T)

single-point energies were obtained using the cc-pVDZ[38–40] and aug-cc-pVDZ basis sets combined with the SBKJ pseudo-potential for the core electrons of Cu. In addition to describing the inner shells of Cu and I with the pseudo-potential, the 3s and 3p orbitals of Cu, and 1s orbital of C and N were frozen in the post-SCF stages of the MP2 and CC calculations. The coupled-cluster computations were performed using the parallel CCSD(T) code described in Refs. 44 and 45, which was obtained by parallelizing the serial CCSD(T) algorithm described in detail in Ref. 46 and implemented in GAMESS(US)[47,48]. Calculations involving the B97-1, B97-2, M06 and TPSS families of functionals, and CCSD(T) were carried out with the GAMESS(US) computational package. All other DFT and MP2 computations were performed with the Firefly program[49].

Results and Discussion

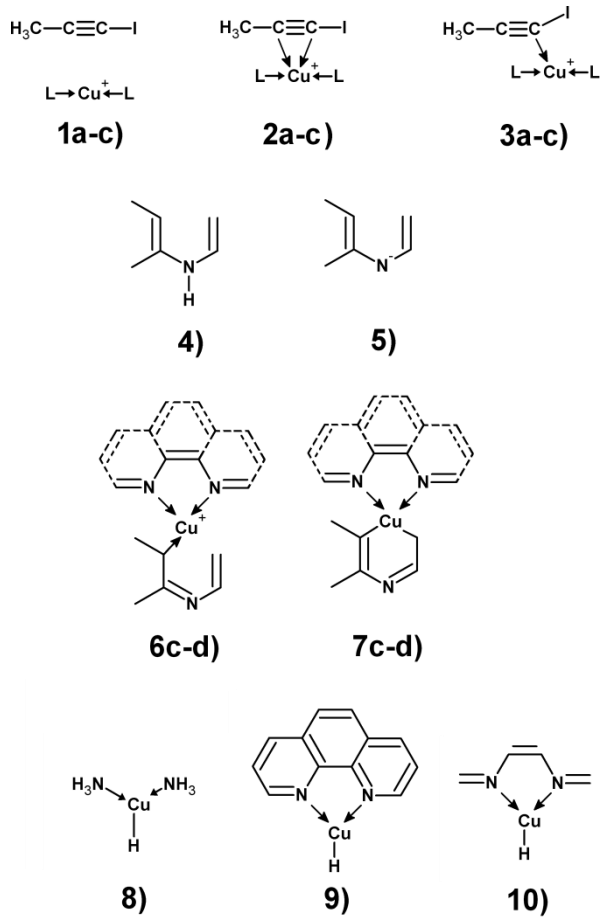

Figure 1: Chemical systems studied in this work. a) L=NH_3; b) L=$N(CH_3)_3$; c) L= phenanthroline; d) L= H_2C=N-CH_2=CH_2-N=CH_2

Complexation of iodoalkynes by N-coordinated Cu^+ complexes (MP2)

We began our study by evaluating the complexation of iodoalkynes by bi-coordinated Cu(I) complexes (Figure 1, structures 1-3). At the MP2 level, formation of the π-bonded complex **2** from the pre-reactional complex **1** is always favored over the σ-bonded adduct **3**, irrespective of the nature of the nitrogen-containing Cu^+ ligands. The influence of the ligands reflects itself on the degree of spontaneity of formation of the

complexes: phenanthroline-ligated Cu^+ binds to the iodoalkyne much more strongly than ammonia-ligated Cu^+, which itself is a better iodoalkyne complexant than $[Cu(N(CH_3)_3)_2]^+$ (Table 1). In the π-bonded complex, the iodoalkyne always lies on the plane defined by the N-Cu-N angle, and the distance between Cu and the halogenated C atom in the alkyne is consistently 0.04-0.05 Å shorter than the other Cu-C bond (Figure 2). Both Cu-C bond lengths are shorter than the 1.97 Å measured experimentally[50,51] in π-complexes of alkynes and N/O-liganded Cu(I).

The structure of the σ-bonded adduct **3** is much more sensitive to the type of Cu^+ ligand used: phenanthroline affords a species (**3c**) where iodine and the halogenated carbon form the basis of a triangle which has the Cu ion as its apex (Figure 2), whereas NH_3 yields a very weakly bound species (**3a**) with very long (2.62 Å) bond between Cu^+ and the halogenated carbon similar to the pre-reactional complex **1a**. No σ-bonded adduct (**3b**) is formed when trimethylamine is used as a Cu^+ ligand. The pre-reactional complexes **1** are generally unremarkable, with the exception of the phenanthroline-ligated Cu^+, where an interaction between iodine and the metal is evident (Table 4).

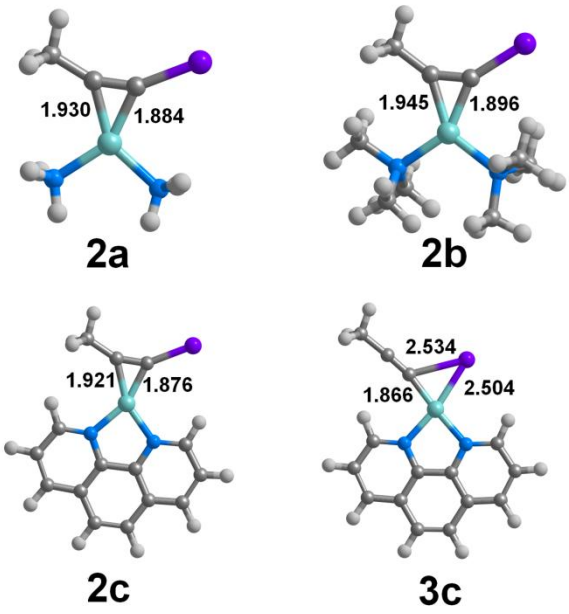

Figure 2: Representative geometries of some Cu^+-iodoalkyne complexes at the MP2/SBKJ-6-31G* level.

Density-functional theory description of complexation of iodoalkynes by N-coordinated Cu^+ complexes

Density-functional studies of these systems afforded broadly similar results to MP2, although with many different details (Tables 1-4). In the Cu-alkyne π-complexes, distances computed by DFT are consistently ~0.1 Å longer than the corresponding MP2 distances, and the Cu-C bonds are less symmetrical than observed with MP2 (bond distances differ by 0.08-0.11 Å between themselves). The electronic influences of the ligands on the interaction energies are, however, well captured by almost all functionals, which clearly replicate the increasing stability of the Cu-alkyne π-complex and the shortening of the Cu-C bonds as the ligand changes from $N(CH_3)_3$ to NH_3 and to phenanthroline observed with MP2. A few functionals predict that in the trimethylamine-liganded Cu-alkyne π-bonded species the Cu-alkyne plane is rotated relative to the N-Cu-N plane (PBE1PW91: 20.2º; PBE0: 21.1º; B3PW91: 21.6º; X3LYP: 23.4º; B3LYP: 23.7º), instead of the coplanarity of the alkyne, Cu and N atoms afforded by all other methods. Surprisingly, the M06-HF functional afforded very poor results, producing a barely-bonded Cu-alkyne π-complex with Cu-C distances above 2.20 Å when NH_3 or phenanthroline were used as ligands, and no complex at all when the ligand was trimethylamine.

The σ-bonded adducts **3** are the most sensitive structures to the details of the DFT functional used. With NH_3 as a ligand (**3a**), two functionals (PBEPW91 and TPSSm) predicted short-bonded σ-bonded adducts, in contrast to the MP2 results and all other

functionals. The σ-bonded adducts obtained with DFT using trimethylamine as Cu-ligand (**3b**) are all of the short-bond type (Table 3), although some variation is seen: B3LYP, X3LYP, B97-1 and B97-2 predict Cu-C distances between 2.15-2.20 Å, whereas the other functionals predict shorter distances, below 2.1 Å. At the BHHLYP and M06-HF levels, like in MP2, these σ-bonded adducts are not stable species in the potential energy surface. In agreement with the MP2 results, phenanthroline-ligated Cu^{+} affords σ-adducts (**3c**) with very short Cu-C bonds (1.86-1.94 Å) for all functionals except M06, M06-HF and BHHLYP.

Analysis of the reaction energies showed large variations (up to 15 kcal.mol^{-1}) in the values predicted by the different density-functionals (Table 1). With the exception of M06-HF and BHHLYP, however, most functionals correctly reproduced the energetic trends predicted by MP2. The best correlations with the MP2 values ($R>0.98$) were obtained for M06-L (errors between 1.3 and 5.8 kcal.mol^{-1}), PBE0 (errors between 6.9 and 12.5 kcal.mol^{-1}) and PBE1PW91 (errors between 6.7 and 13.0 kcal.mol^{-1}) using the BS1 basis set. Addition of diffuse basis functions did not improve the correlation between the DFT functional and MP2 energies, except for the PBEPW91, whose performance with the larger BS2 basis set is comparable to that of PBE0 and PBE1PW91 with the less demanding BS1 basis set.

Table 1: Computed gas-phase model reaction energies. All values in kcal.mol^{-1}. MP2 values were computed with the aug-cc-pVTZ basis set, combined with the SBKJ pseudo-potential for the core electrons on Cu and I. DFT energies were computed with the BS1 basis-set (6-311G(2d,p) for all elements except Cu, which used the s6-31G* basis set). n.a.: not applicable, since the product is not a minimum of the potential energy surface at this theory level.

	MP2	B3LYP	B3PW91	B97-1	B97-2	BHHLYP	M06-HF	M06-L	M06	PBE0	PBE1PW91	PBEPW91	X3LYP
1a→2a	-20.9	-4.5	-8.3	-6.9	-6.1	-0.7	-2.6	-15.0	-7.6	-9.0	-8.6	-12.0	-4.6
1a→3a	-5.2	1.2	2.1	0.9	1.0	0.9	-3.6	-2.0	-1.3	1.6	1.5	1.7	1.2
1b→2b	-11.3	6.3	3.0	2.6	5.3	n.a	n.a	-8.2	1.4	0.4	0.7	-3.2	5.9
1b→3b	n.a.	10.0	8.7	8.6	9.2	n.a	n.a	4.3	4.0	6.8	6.9	5.0	9.7
1c→2c	-36.3	-21.0	-23.7	-23.3	-21.9	-16.0	-8.9	-31.4	-20.6	-24.7	-24.3	-27.7	-21.2
1c→3c	-19.6	-4.4	-7.5	-7.8	-4.2	n.a	n.a	-18.4	n.a	-7.1	-6.6	-18.2	-4.0

Table 2: Selected geometric parameters of complexes of iodoalkyne with $Cu(NH_3)_2^+$. Cu-C distances in Å, angles in degrees.

	1a		**2a**			**3a**		
	Cu-C-I distance	Cu-C-R distance	Cu-C-I distance	Cu-C-R distance	Cu-C-I angle	Cu-C-I distance	Cu-C-R distance	Cu-C-I angle
B3LYP	4.045	4.697	1.954	2.038	130.2	2.832	3.142	97.0
B3PW91	3.934	4.645	1.934	2.010	130.9	2.498	2.905	97.1
B97-1	3.939	4.625	1.936	2.042	128.6	2.764	3.089	96.9
B97-2	4.043	4.700	1.937	2.046	127.9	2.737	3.074	96.0
BHHLYP	3.980	4.651	2.009	2.091	125.8	2.777	3.031	97.0
MP2	3.983	4.639	1.884	1.930	136.3	2.623	2.877	104.5
M06-HF	3.581	4.411	2.354	2.401	115.8	2.641	2.465	98.1
M06-L	3.821	4.561	1.893	1.980	129.9	2.696	3.046	91.7
M06	3.691	4.485	1.946	2.040	125.8	2.617	2.862	96.8
PBE0	3.850	4.583	1.931	2.006	130.1	2.482	2.876	96.1
PBE1PW91	3.85	4.59	1.933	2.009	129.9	2.520	2.904	95.8
PBEPW91	3.87	4.61	1.921	2.001	132.2	2.055	2.78	98.3
TPSSh	3.89	4.63	1.911	2.011	129.9	2.988	3.201	96.4
TPSSm	3.95	4.66	1.908	2.012	130.8	2.081	2.806	98.3
TPSS	3.89	4.63	1.906	2.010	130.7	2.985	3.198	96.4
X3LYP	4.02	4.67	1.953	2.036	129.9	2.790	3.086	97.5

Table 3: Selected geometric parameters of complexes of iodoalkyne with $Cu[N(CH_3)_3]_2^+$. Cu-C distances in Å, angles in degrees. **→1b**: unstable species that spontaneously rearranges to species **1b**; **→2b**: unstable species that spontaneously rearranges to species **2b**

	1b		**2b**			**3b**		
	Cu-C-I distance	Cu-C-R distance	Cu-C-I distance	Cu-C-R distance	Cu-C-I angle	Cu-C-I distance	Cu-C-R distance	Cu-C-I angle
B3LYP	3.986	4.161	1.976	2.076	135.9	2.167	2.572	108.7
B3PW91	3.989	4.166	1.951	2.040	137.4	2.077	2.512	108.4
B97-1	3.892	4.144	1.959	2.043	140.4	2.219	2.592	108.2
B97-2	4.177	4.475	1.964	2.056	139.8	2.211	2.591	108.0
BHHLYP	3.858	4.117		**→1b**			**→1b**	
MP2	2.944	3.089	1.896	1.945	144.4		**→2b**	
M06-HF	2.381	2.509		**→1b**			**→1b**	
M06-L	2.702	2.894	1.910	1.985	141.0	2.02	2.402	110.9
M06	2.640	2.820	1.959	2.049	138.3	2.094	2.563	99.7
PBE0	3.427	3.567	1.947	2.031	137.0	2.087	2.427	109.6
PBE1PW91	3.400	3.537	1.950	2.033	137.2	2.091	2.430	109.5
PBEPW91	3.689	3.847	1.933	2.026	141.0	2.006	2.737	101.8
TPSSh	3.987	4.202	1.934	2.017	141.9	2.029	2.657	103.5
TPSSm	4.101	4.279	1.935	2.022	142.6	2.005	2.702	104.2
TPSS	4.009	4.202	1.931	2.016	142.5	2.003	2.698	103.8
X3LYP	3.821	4.001	1.976	2.073	135.8	2.188	2.566	108.5

Table 4: Selected geometric parameters of complexes of iodoalkyne with Cu(phenanthroline)$^{+}$. Cu-C distances in Å, angles in degrees. →**2c**: unstable species that spontaneously rearranges to species **2c**

	1c		**2c**			**3c**		
	Cu-C-I distance	Cu-I distance	Cu-C-I distance	Cu-C-R distance	Cu-C-I angle	Cu-C-I distance	Cu-C-R distance	Cu-C-I angle
B3LYP	3.538	2.541	1.933	2.007	132.1	1.934	2.995	78.6
B3PW91	3.516	2.514	1.914	1.984	132.8	1.915	2.997	76.6
B97-1	3.488	2.539	1.929	1.994	132.8	1.905	3.023	75.5
B97-2	3.525	2.536	1.928	1.999	132.3	1.951	2.967	80.3
BHHLYP	3.504	2.573	1.970	2.041	128.1		→**2c**	
MP2	3.389	2.449	1.876	1.921	137.7	1.866	3.096	67.4
M06-HF	3.314	2.696	2.243	2.300	115.5		→**2c**	
M06-L	3.520	2.494	1.885	1.948	132.7	1.882	3.020	72.4
M06	3.387	2.500	1.927	1.994	129.3		→**2c**	
PBE0	3.495	2.510	1.912	1.977	132.2	1.922	2.977	77.4
PBE1PW91	3.496	2.512	1.914	1.980	132.1	1.925	2.975	77.6
PBEPW91	3.514	2.493	1.906	1.979	134.0	1.876	3.061	71.1
TPSSh	3.531	2.505	1.904	1.974	133.6	1.873	3.050	70.5
TPSSm	3.554	2.503	1.905	1.979	134.4	1.871	3.077	69.0
TPSS	3.546	2.496	1.902	1.974	134.3	1.865	3.074	68.4
X3LYP	3.535	2.541	1.932	2.005	131.9	1.937	2.982	79.3

Deprotonation of enamines and Cu^+ coordination of the product

Table 5: Computed gas-phase **4→5** reaction energies. All values in kcal.mol^{-1}. MP2 values were computed using the aug-cc-pVTZ basis set, combined with the SBKJ pseudo-potential for the core electrons on Cu. BS1: 6-311G(2d,p) for all elements except Cu, which used the s6-31G* basis set; BS2: 6-311+G(2d,p) for all elements except I and Cu, which used 6-311G(d,p) or aug-cc-pVDZ, respectively.

	BS1	BS2
B3LYP	376.7	371.0
B3PW91	377.5	372.6
B97-1	377.3	371.9
B97-2	379.1	374.0
BHHLYP	381.0	375.5
MP2	367.9	
M06-HF	376.1	370.9
M06-L	374.5	370.8
M06	373.4	368.6
PBE0	377.0	371.8
PBE1PW91	377.2	372.0
PBEPW91	372.8	367.1
TPSSh	377.0	372.0
TPSSm	375.8	370.4
TPSS	375.6	370.4
X3LYP	376.5	370.6

The proposed mechanism for the Cu^{+}-catalyzed synthesis of indoles from aromatic enamines[8] begins with the deprotonation of the substrate and continues with the binding of the complex to the substrate double bond and eventual formation of bidentate complex with the substrate after loss of a proton. We have examined a simplified model of this reaction, where the aromatic ring has been replaced with a simple alkene (Figure 1, structures 4-7). As expected from previous studies of deprotonation of organic molecules[52,53], most density functionals afforded optimized geometries very similar to the MP2 geometry, although the precise energetics of the deprotonation had considerable errors at the BS1 level, which lacks diffuse basis functions (Table 5). The larger BS2 basis set, which does include diffuse basis functions on the heavy atoms, yields a much better description of the anionic, deprotonated species **5**, thereby strongly reducing the absolute error in the energies. PBE1PW91 and M06 emerged as the more appropriate functionals for the description of this deprotonation, with errors below 1 $kcal.mol^{-1}$ when compared to MP2.

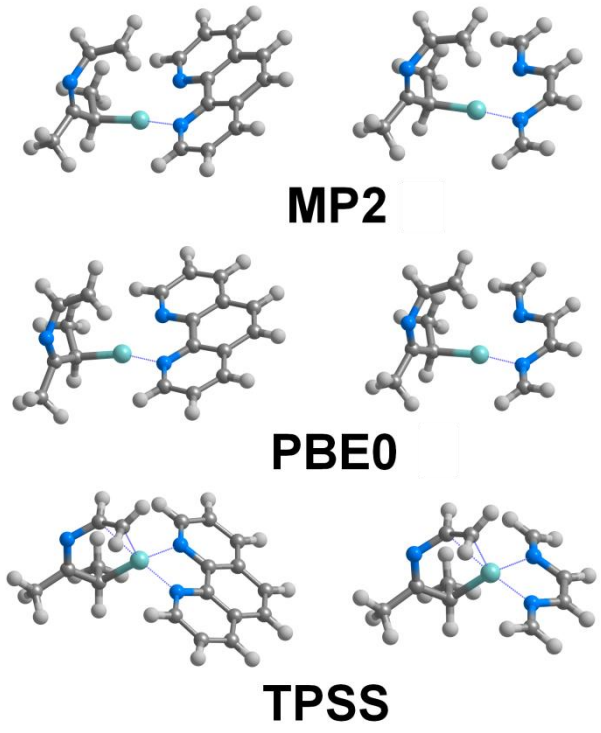

Figure 3: Optimized geometries of **6c** (left) and **6d** (right) using MP2 and different DFT functionals.

The most interesting differences between MP2 and the density functionals arise in the study of the monodentate (**6**) and deprotonated bidentate (**7**) complexes. Unlike MP2 and most functionals, which predict that the nitrogen-containing ligand of Cu^+ in **6** changes its coordination mode from bidentate to monodentate upon complexation with **5**, M06-HF, PBEPW91 and the TPSS family of functionals find a bidentate geometry to be more favorable and predict the formation a π-complex between the Cu^+ ion and the substrate double bond (Table 6 and Figure 3). Upon deprotonation of **6c** to **7c**, very similar geometries are obtained with all methods but M06-HF and (to a lower extent) BHHLYP (Table 7). Surprisingly, the reaction energetics obtained at the MP2/aug-cc-pVTZ and DFT levels of theory differ by very expressive and variable amounts (17-62 $kcal.mol^{-1}$), even when considering the functionals M06-L, PBE0, and PBE1PW91, which provide the best geometric agreement with MP2 (Table 8). At the MP2 level, changing the Cu^+ ligand from phenanthroline, **c,** to the less conjugated analogue **d**, increases the thermodynamic barrier by 9.4 $kcal.mol^{-1}$, whereas the effect at the DFT level is generally smaller (4-8 $kcal.mol^{-1}$ for most functionals). The geometries of **7d** are more sensitive to theory level than those of **7c**, as the Cu^+-nitrogen bonds are considerably less symmetric using DFT than MP2. M06-HF shows the most peculiar behavior among the functionals tested by predicting the reaction to be more favorable with the less-conjugated ligand, which is consistent with the strikingly different geometries obtained with this functional.

The energetic disagreement between MP2 and the tested functionals does not necessarily mean that we have met a failure of density functional theory in this reaction energy, as poor performance of MP2 in the energetics of metal-containing complexes is not unprecedented[54]; we have therefore computed the energies of the **6c→7c** and **6d→7d** reactions using the very high quality CCSD(T) method on the geometries obtained with MP2.

Table 6: Selected geometric parameters of complexes of **5** with Cu^+(phenanthroline) (**6c**) or Cu^+(H_2C=N-CH_2=CH_2-N=CH2) (**6d**). Distances in Å. [a]monodentate N-ligation

	6c		**6d**	
	Cu-C distance	**Cu-N distances**	**Cu-C distance**	**Cu-N distances**
B3LYP	1.965	2.006[a]	1.959	1.994[a]
B3PW91	1.954	1.993[a]	1.950	1.980[a]
B97-1	1.966	2.011[a]	1.962	1.996[a]
B97-2	1.966	2.029[a]	1.959	1.999[a]
BHHLYP	1.978	2.053[a]	1.972	2.039[a]
MP2	1.919	1.940[a]	1.915	1.929[a]
M06-HF	2.123	2.186 / 2.231	2.098	2.206 / 2.236
M06-L	2.024	2.028 / 2.138	1.953	1.974[a]
M06	1.948	1.998[a]	1.949	1.990[a]
PBE0	1.954	1.999[a]	1.948	1.982[a]
PBE1PW91	1.954	1.997[a]	1.949	1.984[a]
PBEPW91	2.023	2.011 / 2.120	2.029	2.037 / 2.145
TPSSh	2.022	2.019 / 2.122	2.022	2.034 / 2.183
TPSSm	2.029	2.018 / 2.114	2.028	2.032 / 2.165
TPSS	2.025	2.011 / 2.105	2.026	2.028 / 2.141
X3LYP	1.963	2.005[a]	1.958	1.994[a]

Table 7: Selected geometric parameters of deprotonated complexes of **5** with Cu^+(phenanthroline) (**7c**) or Cu^+(H_2C=N-CH_2=CH_2-N=CH2) (**7d**). Distances in Å.

	7c			**7d**		
	Cu-CH_2 distance	**Cu-C distance**	**Cu-N distances**	**Cu-CH_2 distance**	**Cu-C distance**	**Cu-N distances**
B3LYP	2.033	1.991	2.057 / 2.065	2.063	1.997	2.022 / 2.282
B3PW91	2.012	1.975	2.019 / 2.035	2.029	1.992	2.008 / 2.172
B97-1	2.015	1.989	2.028 / 2.033	2.037	2.003	2.029 / 2.183
B97-2	2.028	1.984	2.073 / 2.065	2.051	2.002	2.037 / 2.236
BHHLYP	2.056	2.008	2.090 / 2.138	2.175	2.025	2.065 / 2.489
MP2	1.998	1.962	1.966 / 1.971	1.988	1.969	1.974 / 2.001
M06-HF	2.423	2.093	2.394 / 2.289	2.383	2.101	2.298 / 2.345
M06-L	2.012	1.972	2.054 / 2.031	2.034	1.988	2.027 / 2.169
M06	2.013	1.991	2.027 / 2.037	2.065	1.959	1.967 / 2.540
PBE0	2.001	1.970	2.008 / 2.016	2.019	1.988	2.003 / 2.148
PBE1PW91	2.003	1.972	2.012 / 2.020	2.023	1.989	2.005 / 2.159
PBEPW91	2.020	1.975	2.014 / 2.028	2.033	1.994	2.017 / 2.152
TPSSh	2.012	1.981	2.007 / 2.014	2.031	1.998	2.010 / 2.131
TPSSm	2.023	1.988	2.015 / 2.024	2.043	2.003	2.020 / 2.145
TPSS	2.019	1.983	2.008 / 2.016	2.038	1.999	2.013 / 2.132

X3LYP	2.032	1.989	2.054 / 2.062	2.060	1.995	2.020 / 2.273

Table 8: Computed gas-phase model reaction energies. All values in kcal.mol^{-1}. MP2 values were computed with the basis sets shown, combined with the SBKJ pseudo-potential for the core electrons on Cu. DFT energies were computed with the BS1 basis-set (6-311G(2d,p) for all elements except Cu, which used the s6-31G* basis set). CCSD(T) energies were computed using MP2-optimized geometries. In the "Composite" CCSD(T) method, [CCSD(T)-MP2] energies with a given basis set were added to the MP2/aug-cc-pVTZ energies. n.c: not computed due to prohibitive computational cost

	6c→7c	**6d→7d**
MP2/cc-pVDZ	344.5	354.9
MP2/aug-cc-pVDZ	328.4	336.7
MP2/aug-cc-pVTZ	333.2	343.2
B3LYP	374.9	382.4
B3PW91	370.1	378.4
B97-1	372.0	381.4
B97-2	377.4	384.8
BHHLYP	396.0	400.3
M06-HF	395.8	392.8
M06-L	365.2	372.6
M06	375.8	383.8
PBE0	369.9	379.3
PBE1PW91	371.1	380.2
PBEPW91	358.7	359.9
TPSSh	364.0	367.9
TPSSm	367.2	372.9
TPSS	364.5	368.6

X3LYP	375.2	382.7
CCSD(T)/cc-pVDZ//MP2	376.4	391.4
CCSD(T)/aug-cc-pVDZ//MP2	n.c.	375.0
“Composite” CCSD(T)/cc-pVDZ//MP2	365.1	379.7
“Composite” CCSD(T)/aug-cc-pVDZ//MP2	n.c.	381.6

Our CCSD(T) calculations (Table 8) show that these reactions do not represent a case of failure of DFT, but rather an example of poor performance of MP2, which offers a low-order treatment of correlation that may become quite problematic in transition metal chemistry. Removal of diffuse functions in the MP2 computations moves the reaction energies towards the DFT values, though they still remain far below most functionals. Thus, it is quite clear that the basis set, although important, is not the major factor in this discussion, i.e., the difference between MP2 and DFT is mainly related to problems with MP2. On the other hand, the CCSD(T)/cc-pVDZ results changes the MP2/cc-pVDZ energy from 354.9 kcal.mol^{-1} (only 10 kcal.mol^{-1} above MP2/aug-cc-pVTZ, and still well below any of the DFT results) to 391.4 kcal.mol^{-1} (36.5 kcal.mol^{-1} towards DFT values). When using the aug-cc-pVDZ basis set, the CCSD(T) reaction energy is reduced to 375.0 kcal.mol^{-1}, which is in the range of the DFT results.

The ratios of the MP2 and CCSD(T) correlation energies determined with the cc-pVDZ and aug-cc-pVDZ basis sets show that MP2 captures the vast majority of the many-electron correlation effects (about 95-97 %; in the case of the **6c→7c** and **6d→7d** systems). Therefore, the electron correlation effects missed by MP2 within a given basis set may be safely assumed to be properly estimated by forming the difference of the CCSD(T) and MP2 energies determined using a smaller basis set. Thus, in addition to the pure CCSD(T)/cc-pVDZ results, we have performed “Composite” calculations[55], in which the energy is defined as MP2/(aug-cc-pVTZ+SBKJ) + [CCSD(T) - MP2]/(cc-pVDZ+SBKJ). In this case, the majority of the electron correlation is described using the aug-cc-pVTZ basis set and the smaller missing electron correlation (3-5 %) using the cc-pVDZ basis. The “Composite” results

obtained in this way are in the middle of the DFT results (Table 8). This "Composite" approach is stable with respect to the basis set used in the CCSD(T) calculations, since if we calculate the "Composite" energy for the **6d→7d** reaction using the aug-cc-pVDZ basis set in the CCSD(T) portion of the computations, we obtain 381.6 kcal.mol^{-1}, in excellent agreement with the analogous result obtained based on the "Composite" CCSD(T)/cc-pVDZ calculations (379.7 kcal.mol^{-1}). The "Composite" energies of ~365 kcal.mol^{-1} for the **6c→7c** reaction and ~380 kcal.mol^{-1} for the **6d→7d** reaction can be regarded as reasonably converged estimates of the CCSD(T)/aug-cc-pVTZ reaction energies, which may carry an error of up to about 2 kcal.mol^{-1} relative to the pure CCSD(T)/aug-cc-pVTZ calculations, considering the above remarks. The energetic effect of the Cu^+-ligand on the difference of **6d→7d** and **6c→7c** reaction energies (~15 kcal.mol^{-1} at the "Composite" CCSD(T) level) was underestimated by most DFT functionals. B97-1, PBE0 and PBE1PW91 emerged as the functionals which more closely resemble both the "Composite" CCSD(T) values and the ligand effect on the reaction energies.

Evolution of H_2 from Cu^+ hydrides

We next evaluated the ability of DFT functionals to correctly describe the influence of ligands on the redox potential of Cu(I) hydrides **8**, **9** and **10**. The geometries of hydride-free Cu(I) complexes (**8'**,**9'** and **10'**) obtained using MP2 were extremely similar to those obtained with DFT, with the lone exception of the M06-HF functional, which yielded (as in previously described molecules) large differences (>0.10 Å) in key bond-lengths between Cu and its coordinating atoms for all complexes studied. Upon addition of hydride to the Cu(I) systems with conjugated ligands (**9'** and **10'**), both bonds between Cu^+ and its ligand nitrogen atoms increase symmetrically by 0.12 Å at the MP2 level, yielding a tricoordinated Cu ion, whereas hydride addition to $Cu^+(NH_3)_2$ (**8'**) results in the release of one of the ammonia ligands. For the hydride complex **8**, most density-functional theory predicts only slightly longer Cu-H (0.008-0.015 Å) and Cu-N (0.006-0.030 Å) bonds than MP2, but M06-HF again predicts

much larger deviations from the MP2 reference. Roughly half of the tested functionals (B97-1, B97-2, M06, M06-HF, M06-L, TPSS, TPSSh and TPSSm) predict, for the geometries of hydride complexes with conjugated ligands (**9** and **10**), a strikingly different geometry from MP2 and the other functionals, with the ligand bound to the Cu^+ through only one nitrogen atom (Table 9). The predicted reaction energies are, however, very well correlated with the MP2 values for all functionals in spite of the observed differences in the geometric parameters of the Cu^+ hydrides (Table 10). The best performance, as shown by the unity slope of the linear regression of the DFT reaction energies *vs.* the MP2 reference (Table 10, last column), is that of PBEPW91, which matches MP2 almost perfectly after subtracting the average PBEPW91 vs. MP2 error of 2.58 $kcal.mol^{-1}$. M06-L, which has previously been recommended[26] as the best member of the M06 family for transition-metal-containing species, surprisingly had one of the worst performances in this reaction set, as it predicts the reaction energies to vary by more than 30 $kcal.mol^{-1}$ (instead of the 26 $kcal.mol^{-1}$ predicted by MP2) as the Cu^+ ligand changed from ammonia to phenanthroline to $H_2C{=}N{-}CH_2{=}CH_2{-}N{=}CH_2$.

Table 9: Selected geometric parameters of **8'**, **9'**, **10'** and corresponding hydrides (**8**, **9** and **10**). Distances in Å.

	8'		**8**		**9'**		**9**			**10'**		**10**		
	$Cu\text{-}NH_3$	$Cu\text{-}NH_3$	$Cu\text{-}NH_3$	Cu-H	$Cu\text{-}N^1$	$Cu\text{-}N^2$	$Cu\text{-}N^1$	$Cu\text{-}N^2$	Cu-H	$Cu\text{-}N^1$	$Cu\text{-}N^2$	$Cu\text{-}N^1$	$Cu\text{-}N^2$	Cu-H
B3LYP	1.922	1.922	1.976	1.495	2.000	1.998	2.185	2.182	1.515	2.015	2.014	2.197	2.195	1.511
B3PW91	1.912	1.912	1.961	1.495	1.985	1.984	2.149	2.148	1.517	2.000	1.999	2.162	2.159	1.514
B97-1	1.924	1.924	1.975	1.499	1.997	2.007	2.378	2.037	1.517	2.023	2.009	2.470	2.025	1.513
B97-2	1.926	1.926	1.976	1.499	2.000	2.011	2.370	2.046	1.516	2.030	2.015	2.448	2.035	1.513
BHHLYP	1.934	1.934	1.981	1.501	2.022	2.022	2.211	2.208	1.522	2.039	2.039	2.222	2.219	1.519
MP2	1.895	1.895	1.929	1.487	1.992	1.992	2.118	2.115	1.503	2.009	2.008	2.123	2.119	1.501
M06-HF	2.030	2.030	2.070	1.567	2.088	2.089	2.215	2.294	1.593	2.102	2.098	2.249	2.246	1.593
M06-L	1.912	1.912	1.968	1.500	1.972	1.991	2.338	2.000	1.521	2.008	1.979	2.304	1.985	1.522
M06	1.902	1.902	1.956	1.500	1.980	1.986	2.278	2.074	1.519	2.001	1.993	2.482	2.002	1.512
PBE0	1.911	1.911	1.957	1.498	1.987	1.986	2.148	2.146	1.520	2.001	2.000	2.158	2.155	1.516
PBE1PW91	1.912	1.912	1.959	1.497	1.989	1.988	2.152	2.150	1.519	2.003	2.002	2.163	2.160	1.516
PBEPW91	1.908	1.908	1.958	1.498	1.968	1.966	2.117	2.114	1.52	1.979	1.978	2.125	2.121	1.519

TPSSh	1.914	1.914	1.948	1.500	1.973	1.986	2.297	1.998	1.521	1.999	1.982	2.349	1.991	1.517
TPSSm	1.918	1.918	1.963	1.502	1.968	1.984	2.297	1.990	1.525	1.996	1.977	2.357	1.983	1.521
TPSS	1.913	1.913	1.958	1.500	1.962	1.978	2.284	1.984	1.523	1.989	1.971	2.336	1.978	1.519
X3LYP	1.920	1.920	1.972	1.494	1.999	1.997	2.182	2.180	1.515	2.014	2.013	2.194	2.192	1.511

Table 10: Computed gas-phase model reaction energies. All values in kcal.mol^{-1}. MP2 values were computed with the aug-cc-pVTZ basis set, combined with the SBKJ pseudo-potential for the core electrons on Cu. DFT energies were computed with the BS1 basis-set (6-311G(2d,p) for all elements except Cu, which used the s6-31G* basis set)

	8 + H^+ → **8'** + H_2	**9** + H^+ → **9'** + H_2	**10** + H^+ → **10'** + H_2	R^2	Regression slope
MP2	-258.6	-242.5	-232.7		
B3LYP	-259.3	-246.0	-237.0	0.999	0.86
B3PW91	-261.6	-247.6	-239.0	1.000	0.87
B97-1	-260.6	-245.9	-236.8	1.000	0.92
B97-2	-263.1	-249.7	-240.7	0.999	0.86
BHHLYP	-262.9	-251.1	-243.0	0.999	0.76
M06-HF	-267.8	-258.8	-253.0	1.000	0.57
M06-L	-257.0	-237.1	-226.7	0.998	1.18
M06	-257.1	-243.0	-233.0	0.998	0.93
PBE0	-260.2	-245.7	-237.2	1.000	0.89

PBE1PW91	-260.3	-245.8	-237.3	1.000	0.89
PBEPW91	-256.0	-239.1	-230.1	0.999	1.00
TPSS	-262.8	-244.8	-236.1	0.997	1.04
TPSSh	-263.7	-247.0	-238.3	0.998	0.98
TPSSm	-263.2	-245.8	-237.0	0.998	1.02
X3LYP	-258.5	-245.1	-236.1	0.999	0.86

Conclusions

Our study of the relative energies and geometries of alkyne-bonded Cu^+-complexes showed that the π-bonded species **2** is described in approximately the same way by all functionals and MP2. In contrast, several functionals (BHHLYP, PBEPW91, TPSSm) afford, for the σ–bonded species **3**, unusual geometries that do not agree either with other functionals or with MP2. The relative effect of the Cu^+ ligand on the relative strength of the Cu^+-alkyne interactions, and the strong preference for the π-bonding mode is captured by all functionals, although the absolute values of the interactions differ significantly between functionals and MP2. The best energetic correlations with MP2 are obtained with PBE0, M06-L and PBE1PW91, which also provide reliable geometries. PBE0 and PBE1PW91 also afford the best agreement with the high-level CCSD(T) computations of the deprotonation energies of Cu^+-coordinated eneamine **6**, a system where the much more expensive MP2 method strongly disagrees with CCSD(T). PBEPW91 and (again) PBE0 emerged as the most suitable functionals for the study of the energetics and geometries of Cu^+ hydrides **8**, **9**, and **10**, while at the same time correctly capturing the influence of the Cu^+ ligands on the reactivity. The consistently good performance of the hybrid functional PBE0 in this varied set of reactions recommends its use as a suitable "default" choice for the study of Cu^+-catalyzed reactions. The related functionals PBEPW91 and PBE1PW91, which differ from PBE0 on the use of the non-local term from the Perdew1991 correlation functional instead of the Perdew-Burke-Ernzerhof1996 correlation functional and (in the case of PBEPW91) in the absence of Hartree Fock exchange, also behave very satisfactorily in the subset of Cu^+-based reactions.

Acknowledgments: Research at REQUIMTE is supported by Fundação para a Ciência e a Tecnologia through grant no. PEst-C/EQB/LA0006/2011. This work has been financed by FEDER through Programa Operacional Factores de Competitividade – COMPETE and by Portuguese Funds through FCT – Fundação para a Ciência e a Tecnologia under project PTDC/QUI-QUI/111288/2009. This work

has also been supported by the Chemical Sciences, Geosciences and Biosciences Division, Office of Basic Energy Sciences, Office of Science, U.S. Department of Energy (Grant No. DE-FG02-01ER15228; P.P.). Useful discussions with Professor Wei Li and Mr. Jared A. Hansen are gratefully appreciated, too.

Supporting Information Geometries and energies of every molecule optimized with each density functional and with MP2.

References

(1) Miyaura, N.; Suzuki, A. *Chem. Rev.* **1995**, *95*, 2457–2483.

(2) Cui, X.; Burgess, K. *Chem. Rev.* **2005**, *105*, 3272–3296.

(3) Seregin, I. V; Gevorgyan, V. *Chem. Soc. Rev.* **2007**, *36*, 1173–1193.

(4) Negishi, E. *Bull. Chem. Soc. Jpn.* **2007**, *80*, 233–257.

(5) Bernini, R.; Fabrizi, G.; Sferrazza, A.; Cacchi, S. *Angew. Chem. Int. Ed.* **2009**, *48*, 8078–8081.

(6) Hein, J. E.; Tripp, J. C.; Krasnova, L. B.; Sharpless, K. B.; Fokin, V. V *Angew. Chem. Int. Ed.* **2009**, *48*, 8018–8021.

(7) Das, J. P.; Chechik, H.; Marek, I. *Nat. Chem.* **2009**, *1*, 128–132.

(8) Himo, F.; Lovell, T.; Hilgraf, R.; Rostovtsev, V. V; Noodleman, L.; Sharpless, K. B.; Fokin, V. V *J. Am. Chem. Soc.* **2005**, *127*, 210–216.

(9) Cantillo, D.; Ávalos, M.; Babiano, R.; Cintas, P.; Jiménez, J. L.; Palacios, J. C. *Org. Biomol. Chem.* **2011**, *9*, 2952–2958.

(10) Sousa, S. F. S. F.; Fernandes, P. A.; Ramos, M. J. J. *J. Phys. Chem. A* **2007**, *111*, 10439–10452.

(11) Becke, A. D. *J. Chem. Phys.* **1993**, *98*, 5648–5652.

(12) Lee, C.; Yang, W.; Parr, R. G. *Phys. Rev. B* **1988**, *37*, 785–789.

(13) Hertwig, R. H.; Koch, W. *J. Comput. Chem.* **1995**, *16*, 576–585.

(14) Perdew, J. P. In *Electronic Structure of Solids '91*; Ziesche, P.; Eschrig, H., Eds.; Akademie Verlag: Berlin, 1991; Vol. 17, pp. 11–20.

(15) Perdew, J. P.; Burke, K.; Ernzerhof, M. *Phys. Rev. Lett.* **1996**, *77*, 3865–3868.

(16) Hamprecht, F. A.; Cohen, A. J.; Tozer, D. J.; Handy, N. C. *J. Chem. Phys.* **1998**, *109*, 6264–6271.

(17) Wilson, P. J.; Bradley, T. J.; Tozer, D. J. *J. Chem. Phys.* **2001**, *115*, 9233–9242.

(18) Becke, A. D. *Phys. Rev. A* **1988**, *38*, 3098–3100.

(19) Adamo, C.; Barone, V. *J. Chem. Phys.* **1999**, *110*, 6158–6170.

(20) Xu, X.; Zhang, Q.; Muller, R. P.; Goddard, W. A. *J. Chem. Phys.* **2005**, *122*, 014105.

(21) Tao, J. M.; Perdew, J. P.; Staroverov, V. N.; Scuseria, G. E. *Phys. Rev. Lett.* **2003**, *91*, 146401.

(22) Staroverov, V. N.; Scuseria, G. E.; Tao, J. M.; Perdew, J. P. *J. Chem. Phys.* **2004**, *120*, 6898–6911.

(23) Perdew, J. P.; Ruzsinszky, A.; Tao, J.; Csonka, G. I. G.; Scuseria, G. E. *Phys. Rev. A* **2007**, *76*, 042506.

(24) Zhao, Y.; Truhlar, D. G. *J. Chem. Phys.* **2006**, *125*, 194101.

(25) Staroverov, V. N.; Scuseria, G. E.; Tao, J. M.; Perdew, J. P. *J. Chem. Phys.* **2003**, *119*, 12129–12137.

(26) Zhao, Y.; Truhlar, D. G. *Theor. Chem. Acc.* **2007**, *120*, 215–241.

(27) Zhao, Y.; Truhlar, D. G. *J. Phys. Chem. A* **2006**, *110*, 13126–13130.

(28) Baker, J.; Kessi, A.; Delley, B. *J. Chem. Phys.* **1996**, *105*, 192–212.

(29) Ditchfield, R.; Hehre, W. J.; Pople, J. A. *J. Chem. Phys.* **1971**, *54*, 724–728.

(30) Hehre, W. J.; Ditchfield, R.; Pople, J. A. *J. Chem. Phys.* **1972**, *56*, 2257–2261.

(31) Stevens, W. J.; Krauss, M.; Basch, H.; Jasien, P. G. *Can. J. Chem.* **1992**, *70*, 612–630.

(32) Krishnan, R.; Binkley, J. S.; Seeger, R.; Pople, J. A. *J. Chem. Phys.* **1980**, *72*, 650–654.

(33) Hariharan, P. C.; Pople, J. A. *Theor. Chim. Acta* **1973**, *28*, 213–222.

(34) Frisch, M. J.; Pople, J. A.; Binkley, J. S. *J. Chem. Phys.* **1984**, *80*, 3265–3269.

(35) Swart, M.; Güell, M.; Luis, J. M.; Solà, M. *J. Phys. Chem. A* **2010**, *114*, 7191–7197.

(36) Clark, T.; Chandrasekhar, J.; Spitznagel, G. W.; Schleyer, P. V. R. *J. Comput. Chem.* **1983**, *4*, 294–301.

(37) Glukhovtsev, M. N.; Pross, A.; McGrath, M. P.; Radom, L. *J. Chem. Phys.* **1995**, *103*, 1878–1885.

(38) Balabanov, N. B.; Peterson, K. A. *J. Chem. Phys.* **2005**, *123*, 064107.

(39) Peterson, K. A.; Shepler, B. C.; Figgen, D.; Stoll, H. *J. Phys. Chem. A* **2006**, *110*, 13877–13883.

(40) Dunning, T. H. *J. Chem. Phys.* **1989**, *90*, 1007–1023.

(41) Kendall, R. A.; Dunning, T. H.; Harrison, R. J. *J. Chem. Phys.* **1992**, *96*, 6796–6806.

(42) Čížek, J. *J. Chem. Phys.* **1966**, *45*, 4256–4267.

(43) Raghavachari, K.; Trucks, G. W.; Pople, J. A.; Head-Gordon, M. *Chem. Phys. Lett.* **1989**, *157*, 479–483.

(44) Olson, R. M.; Bentz, J. L.; Kendall, R. A.; Schmidt, M. W.; Gordon, M. S. *J. Chem. Theory Comput.* **2007**, *3*, 1312–1328.

(45) Bentz, J. L.; Olson, R. M.; Gordon, M. S.; Schmidt, M. W.; Kendall, R. A. *Comput. Phys. Commun.* **2007**, *176*, 589–600.

(46) Piecuch, P.; Kucharski, S. A.; Kowalski, K.; Musiał, M. *Comput. Phys. Commun.* **2002**, *149*, 71–96.

(47) Schmidt, M. W.; Baldridge, K. K.; Boatz, J. A.; Elbert, S. T.; Gordon, M. S.; Jensen, J. H.; Koseki, S.; Matsunaga, N.; Nguyen, K. A.; Su, S.; Windus, T. L.; Dupuis, M.; Montgomery, J. A. *J. Comput. Chem.* **1993**, *14*, 1347–1363.

(48) Gordon, M.; Schmidt, M. In *Theory and Application of Computational Chemistry: The First Forty Years*; Dykstra, C. E.; Frenking, G.; Kim, K. S.; Scuseria, G. E., Eds.; Elsevier: Amsterdam, 2005; pp. 1167 – 1189.

(49) A. A. Granovsky PC GAMESS/Firefly version 7.1.G http://classic.chem.msu.su/gran/gamess/index.html.

(50) Thompson, J. S.; Bradley, A. Z.; Park, K.-H.; Dobbs, K. D.; Marshall, W. *Organometallics* **2006**, *25*, 2712–2714.

(51) Dias, H. V. R.; Flores, J. A.; Wu, J.; Kroll, P. *J. Am. Chem. Soc.* **2009**, *131*, 11249–11255.

(52) Silva, P. J.; Ramos, M. J. *Comput. Theor. Chem.* **2011**, *966*, 120–126.

(53) Brás, N. F.; Perez, M. A. S.; Fernandes, P. A.; Silva, P. J.; Ramos, M. J. *J. Chem. Theory Comput.* **2011**, *7*, 3898–3908.

(54) Ke, Z.; Cundari, T. R. *Organometallics* **2010**, *29*, 821–834.

(55) Ge, Y.; Gordon, M. S.; Piecuch, P.; Włoch, M.; Gour, J. R. *J. Phys. Chem. A* **2008**, *112*, 11873–11884.